Performance in Different Failure Conditions of the Predictor-Corrector Neural Controller within the NASA IFCS F-15 WVU Simulator

M.Battipede[+], P.Gili[*] , M.R. Napolitano[#], M.G. Perhinschi[#], G. Campa[#]
* Department of Aeronautical and Space Engineering, Polytechnic of Turin, Turin, Italy
# Department of Mechanical and Aerospace Engineering,
West Virginia University, Morgantown, WV 26506/6106
+ Mechanics Department, Polytechnic of Turin, Turin, Italy

Abstract

The objective of this paper is to present results from the evaluation of a neural control scheme implemented within the NASA IFCS F-15 project. In particular, the neural network controller is based on an adaptive *predictor-corrector* control strategy. The study is conducted within the WVU IFCS F-15 simulation environment, which enables to evaluate a wide range of failure scenarios. Analysis of the controller performance is performed in situations where the state variables vary within a wide portion of the flight envelope and in different failure conditions. Post failure performance evaluation concerns maneuvers accomplished both with the pilot-in-the-loop and with pre-recorded reference signals. Failure test-cases are grouped in three categories: actuator lockage at an imposed deflection, actuator lockage at the current deflection, missing of a control surface portion. Results demonstrate the capability of the neural controller in dealing with slight and hazardous damages.

1. Introduction

The main objective of the *Intelligent Flight Control System* (IFCS) F-15 program[1] is to develop and evaluate through flight tests innovative flight control schemes, allowing the pilot to recover from primary control surface failures, which are major threats to flight safety.

The control scheme described in this paper is one of the 3 methods proposed by the West Virginia University (WVU) team within the *Gen 2* NASA IFCS project (Figure 1). The common feature of the 3 WVU schemes is that they are all based on neural algorithms, however neural networks (NN) are used in different ways. The first approach is based on the Non Linear Dynamic Inversion (NLDI) technique[2],[3] augmented with a pre-trained neural network (PTNN), providing the values of the aerodynamic and stability derivatives within the whole flight envelope. The second approach features a robust controller based on the Stochastic Optimal Feedforward and Feedback Technique[1] (SOFFT), which belongs to the class of State Feedback Linear Quadratic Optimal Control approaches. In addition, the SOFFT controller is augmented with a neural network to compensate errors due to system uncertainties and/or failures on primary control surfaces.

The third approach, outlined in this paper, takes advantage of the NN capabilities in performing system identification. In particular, the control activity is handled by two adaptive neural entities which identify the forward and the inverse F15 model and are connected according to the *predictor-corrector* scheme[4]. The identification of the forward dynamics of the plant is accomplished to estimate on-line the plant Jacobian, which is used in the inverse model adaptation process to implement the back propagation through the model.

In previous efforts this control architecture has been successfully adopted by the first two authors to implement a fault-tolerant Multi-Input-Multi-Output (MIMO) neural adaptive rate damping autopilot for a nonlinear H-106 helicopter model[5]. In this study the controller is used as a Control Augmentation System (CAS), with the reference model tracking task, within the WVU IFCS F-15 simulation environment. Differently from the previous application, the number of control channels (lat, lon, dir) are less than the number of the commanded surfaces (collective and differential stabilators, differential ailerons, differential canards, collective rudders). This implies that a command distribution action must be accomplished within the control strategy.

2 Control Strategy

As shown in Figure 2 desired handling qualities are set through a reference model. Flight commands are generated by the pilot through longitudinal and lateral stick ($\delta_{lon_{stick}}$, $\delta_{lat_{stick}}$) and pedals ($\delta_{dir_{pedal}}$). These displacement commands are converted[3],[6]-[8] into roll rate, aerodynamic normal and lateral acceleration commands (p_{cmd} , $n_{z_{cmd}}$, $n_{y_{cmd}}$) through stick and pedal gains (K_{lat}, K_{lon}, K_{dir}). Afterwards these commands are transformed into corresponding roll, pitch, and yaw rate commands:

$$\begin{aligned} p_{com} &= p_{cmd} \\ q_{com} &= \frac{g}{V_t} n_{z_{cmd}} \\ r_{com} &= \frac{g}{V_t} \cdot \left(n_{y_{cmd}} + \sin\phi \right) \end{aligned} \qquad (1)$$

The reference model provides filtered angular rate (p_{ref}, q_{ref}, r_{ref}) and angular acceleration commands ($\dot{p}_{ref}$, $\dot{q}_{ref}$, $\dot{r}_{ref}$). For this purpose, first order roll rate and second order pitch and yaw rate transfer functions have been used. The reference signals are processed by the neural controller, which calculates the required control signals. Before feeding the actuators, the control signals are reallocated as follows: the pitch control channel signal moves the collective stabilators, the roll channel acts on the differential ailerons and on the differential stabilators,

the yaw control channel commands the collective rudder and the differential canards. Collective canard deflections are scheduled as a function of the Mach number and the angle-of-attack.

The control scheme is based on the *reference model direct inverse* scheme (also known as *predictor-corrector*). As shown in Figure 2, the plant emulator represents the forward model while the controller action is carried out by the inverse model. The forward and the inverse models have both three input variables and three outputs as they identify the direct dynamic response of angular rates (*p, q, r*) to command inputs (δ_{lat}, δ_{lon}, δ_{dir}) and viceversa. The forward model consists of three Multi-Input-Single-Output (MISO) networks connected in a parallel structure, whereas the inverse model features a SISO network for the longitudinal channel (*q*) and two MISO networks for the lateral and directional channels (*p, r*). This architecture has been selected as a result of a tradeoff between the requirement of suppling exhaustive information to each network and the necessity of minimizing the dimensions of the input/output relationships to the neural schemes. Each NN is Multi Layer Perceptron (MLP) with a single hidden layer which implements the identification of NARX (Neural Auto Regressive with eXternal inputs) systems according to the following scheme:

$$\begin{aligned} \mathbf{y} &= f_{NNfwr}(\phi_{fwr}) \\ \mathbf{u} &= f_{NNinv}(\phi_{inv}) \end{aligned} \qquad (2)$$

with the regressor vector ϕ shown in table 1, where the blocks outlined by the dashed lines are repeated in sequence depending on the number of the system inputs.

Table 1 Regressor vector structure.

ϕ_{fwr}	ϕ_{inv}
$y_{1\,ref}$ (k+1)	y(k)
⋮	⋮
y_1 (k-n)	y(k-n)
u (k-1)	u_1 (k-1)
⋮	⋮
u (k-n)	u_1 (k-n)

Unlike previous implementations of the *predictor-corrector* scheme, the inverse model has no direct feedback, meaning that the NN input vector is independent from the calculated output. Actually the input signals *u(k-1), u(k-2), ..., u(k-n+1)* (with *n* = network order) are provided by a linear inverse model, which feeds the neural system with an estimation of the plant input at the previous time steps $(\delta_{lat}, \delta_{lon}, \delta_{dir})_{lin}$ according to the following equation:

$$\begin{bmatrix} \delta_{lat} \\ \delta_{lon} \\ \delta_{dir} \end{bmatrix}_{lin} = B^{-1} \begin{bmatrix} \dot{p}_{ref} - L_1 \\ \dot{q}_{ref} - M_1 \\ \dot{r}_{ref} - N_1 \end{bmatrix} \qquad (3)$$

where B is the state space system control matrix defined as:

$$B = \begin{bmatrix} b_1 & 0 & b_3 \\ 0 & b_5 & 0 \\ b_7 & 0 & b_9 \end{bmatrix} \qquad (4)$$

Precisely:

$$b_1 = \bar{q}Sb\frac{I_{xz}\left(\frac{C_{n_{\delta_{ds}}}}{2}+C_{n_{\delta_a}}\right)+I_z\left(\frac{C_{l_{\delta_{ds}}}}{2}+C_{l_{\delta_a}}\right)}{I_xI_z-I_{xz}^{\,2}} \qquad (5)$$

$$b_3 = \bar{q}Sb\frac{I_{xz}\left(C_{n_{\delta_r}}-C_{n_{\delta_{dc}}}\right)+I_z\left(C_{l_{\delta_r}}-C_{l_{\delta_{dc}}}\right)}{I_xI_z-I_{xz}^{\,2}} \qquad (6)$$

$$b_5 = \frac{C_{m_{\delta_s}}\bar{q}S\bar{c}}{I_y} \qquad (7)$$

$$b_7 = \bar{q}Sb\frac{I_{xz}\left(\frac{C_{l_{\delta_{ds}}}}{2}+C_{l_{\delta_a}}\right)+I_x\left(\frac{C_{n_{\delta_{ds}}}}{2}+C_{n_{\delta_a}}\right)}{I_xI_z-I_{xz}^{\,2}} \qquad (8)$$

$$b_9 = \bar{q}Sb\frac{I_{xz}\left(C_{l_{\delta_r}}-C_{l_{\delta_{dc}}}\right)+I_x\left(C_{n_{\delta_r}}-C_{n_{\delta_{dc}}}\right)}{I_xI_z-I_{xz}^{\,2}} \qquad (9)$$

where the aerodynamic and control derivatives are relative to trim conditions and are kept constant even in non nominal conditions.

The terms (L_1, M_1, N_1) are the actual plant acceleration contributions, which are functions of the inertial and geometric aircraft characteristics as well as the actual angular rates and aerodynamic angles:

$$L_1 = \frac{1}{I_xI_z-I_{xz}^{\,2}}\left\{\left[pqI_{xz}\left(I_x-I_y+I_z\right)-qr\left(I_z^{\,2}-I_yI_z+I_{xz}^{\,2}\right)\right]+ \bar{q}SbI_{xz}\left[C_{n_\beta}\beta+\frac{b}{2V_t}\left(C_{n_p}p+C_{n_r}r\right)\right]+\bar{q}SbI_z\left[C_{l_\beta}\beta+\frac{b}{2V_t}\left(C_{l_p}p+C_{l_r}r\right)\right]\right\} \qquad (10)$$

$$M_1 = \frac{1}{I_y}\left\{\left[-rp\left(I_x-I_z\right)-I_{xz}\left(p^2-r^2\right)\right]+ \bar{q}S\bar{c}\left[C_{m_u}\frac{u}{V_t}+C_{m_\alpha}\alpha+\frac{\bar{c}}{2V_t}C_{m_q}q\right]+\bar{q}S\bar{c}\left[C_{m_{\delta c}}\delta_{can}\right]\right\} \qquad (11)$$

$$N_1 = \frac{1}{I_xI_z-I_{xz}^{\,2}}\left\{\left[-qrI_{xz}\left(I_x-I_y+I_z\right)-pq\left(I_xI_y-I_x^{\,2}-I_{xz}^{\,2}\right)\right]+ \bar{q}Sb\left\{I_{xz}\left[\bar{C}_{l_\beta}\beta+\frac{b}{2V_t}\left(\bar{C}_{l_p}p+\bar{C}_{l_r}r\right)\right]+I_x\left[\bar{C}_{n_\beta}\beta+\frac{b}{2V_t}\left(\bar{C}_{n_p}p+\bar{C}_{n_r}r\right)\right]\right\}\right\} \qquad (12)$$

The neural inverse model is fed by the linear inverse model and filters the signals compensating for nonlinearities, modeling errors, model uncertainties and the dynamic modifications due to failures and non-nominal flight conditions. The results will show how the neural network activity increases as a consequence of some of the events mentioned above.

Avoiding the direct feedback of the NN output decreases the risk of oscillations during transient phases

and allows greater time steps, which, in turn, reduces the simulation time.

2.1. Neural Network Training Algorithm

The forward and the inverse models are pre-trained using the back-propagation technique featuring the Levenberg-Marquardt method[13].

To make the controller adaptive and fault tolerant, the forward and the inverse model must be trained on-line. The error functions which are minimized for the forward and the inverse model on-line training are respectively:

$$\boldsymbol{E}_m = \tfrac{1}{2}\left(\boldsymbol{y}-\hat{\boldsymbol{y}}\right)^T \boldsymbol{K}_{p_m}\left(\boldsymbol{y}-\hat{\boldsymbol{y}}\right) \qquad (13)$$

$$\boldsymbol{E}_c = \tfrac{1}{2}\left(\boldsymbol{y}_{ref}-\boldsymbol{y}\right)^T \boldsymbol{K}_{p_c}\left(\boldsymbol{y}_{ref}-\boldsymbol{y}\right) \qquad (14)$$

The on-line training algorithm belongs to the Recursive Identification methods category and is basically an extension of the *Recursive Pseudolinear Regression* (RPLR) algorithm[14]. This technique is based on the step by step updating of the $\boldsymbol{\Theta}_{fw}$ and $\boldsymbol{\Theta}_{in}$ vectors, which group in vector shape respectively the couples of matrices $\boldsymbol{W}1_{fw}$, $\boldsymbol{W}2_{fw}$ and $\boldsymbol{W}1_{in}$, $\boldsymbol{W}2_{in}$.

Omitting subscripts for simplicity, the equations below represent the k^{th} time step of the RPLR algorithm:

$$\begin{aligned}
&\mathbf{K}(k) = \mathbf{P}(k-1)\boldsymbol{\Psi}(k)\left[\lambda \boldsymbol{I} + \boldsymbol{K}_p \boldsymbol{\Psi}^T(k)\mathbf{P}(k-1)\boldsymbol{\Psi}(k)\right]^{-1}\\
&\boldsymbol{\Theta}(k) = \boldsymbol{\Theta}(k-1) + \mathbf{K}(k)\boldsymbol{K}_p \boldsymbol{e}(k)\\
&\bar{\mathbf{P}}(k) = \frac{1}{\lambda}\left[\boldsymbol{I} - \mathbf{K}(k)\boldsymbol{K}_p\boldsymbol{\Psi}^T(k)\right]\mathbf{P}(k-1)\\
&\mathbf{P}(k) = \frac{\alpha_{max}-\alpha_{min}}{tr\left(\bar{\mathbf{P}}(k)\right)}\bar{\mathbf{P}}(k) + \alpha_{min}\boldsymbol{I}
\end{aligned} \qquad (15)$$

applied according to the *constant-trace* technique. The $\boldsymbol{\Psi}$ matrix determines the gradient descent direction; for the forward model it is simply:

$$\boldsymbol{\Psi}_{fw_m}(k) = -\nabla_{\boldsymbol{\Theta}_{fw_m}} \boldsymbol{e}_{\hat{y}_m}(k) = \nabla_{\boldsymbol{\Theta}_{fw_m}} \hat{\boldsymbol{y}}_m(k) \qquad (16)$$

with m = 1,...,3, while for the inverse model it is:

$$\begin{aligned}
\boldsymbol{\Psi}_{in_m}(k) &= -\nabla_{\boldsymbol{\Theta}_{in_m}} \boldsymbol{e}_{c_m}(k) \cong \nabla_{\boldsymbol{\Theta}_{in_m}} \hat{\boldsymbol{y}}_m(k) = \\
&= \nabla_{\boldsymbol{u}_{m(k-1)}} \hat{\boldsymbol{y}}_m(k) \cdot \left(\nabla_{\boldsymbol{\Theta}_{in_m}} \boldsymbol{u}_m(k-1)\right)
\end{aligned} \qquad (17)$$

with m = 1,...,3 and where the generic (j,i) element can be written as follows:

$$\boldsymbol{\Psi}_{in_m}(j,i) = \frac{\partial \hat{\boldsymbol{y}}(i)}{\partial \boldsymbol{\Theta}_{in_m}(j)} = \frac{\partial \hat{\boldsymbol{y}}(i)}{\partial \boldsymbol{u}_m}\frac{\partial \boldsymbol{u}_m}{\partial \boldsymbol{\Theta}_{in_m}(j)} \qquad (18)$$

3. Aircraft Model and Simulation Environment

WVU researchers developed a simulation environment[11] based on a nonlinear approximate model of the F-15 aircraft. This model is derived from a Fortran code of a high performance military aircraft distributed by NASA to academic institutions within the 1990 AIAA GNC Design Challenge[12]. The aerodynamic and thrust characteristics are provided through 42 look-up tables, that is 16 tables for the longitudinal dynamics as functions of Mach number, angle of attack and stabilator deflections; 20 tables for the latero-directional dynamics as functions of Mach number, angle of attack, sideslip angle and rudder; 2 tables for engine thrust and fuel flow as functions of Mach number and altitude. Additional look-up tables have been added for the modeling of the canard surfaces on the IFCS F-15 aircraft.

The simulation package is based on the *Flight Dynamics and Control* (FDC) toolbox[13] which is a graphical software environment within Matlab/Simulink. For graphic display and pilot interaction the dynamic model is interfaced with the *Aviator Visual Design Simulator* (AVDS) simulation package[14]. Particularly, the aircraft dynamic model is flown through a joystick device; however, pre-loading of command histories is also possible. In the open loop mode, the inputs given through the joystick are supplied directly to the stabilators, ailerons and rudders actuators, while the collective canard deflection is scheduled as a function of the Mach number and the angle-of-attack.

4 Failure modeling

A failure modeling stategy has been developed and applied for longitudinal, lateral and directional control surface blockage and partial destruction[15],[16]. The method is based on the assumption that when a control device failure occurs, an alteration of the aerodynamic forces and moments results which is equivalent to a net loss of "aerodynamic efficiency". The contribution of each individual control device to the total external forces and moments is isolated and expressed in terms of a single parameter which can be varied during the simulation.

4.1 Actuator blockage

A 'control surface blockage' implies that, after the failure occurrence at time t_{f1}, the deflection of the control surface is no longer controllable since it either remains fixed at the value corresponding to t_{f1} or at a value reached shortly after t_{f1} (which is not a commanded position but a result of the failure). This behavior mainly characterizes a failure of the actuator or an actuator related mechanisms. A failure involving a blockage of the control surface at a fixed deflection value does not alter the aerodynamic properties of the control surface.

4.2. Missing surface

Of different nature is the 'destruction type failure', which means that the "aerodynamic efficiency" of the control surface is deteriorated starting at the failure occurring moment t_{f2}. A surface damage parameter s_d describes the importance of the failure by means of the ratio between the efficiency parameter after and before the failure occurring moment.

$$\left(\mathrm{s_d}\right)_{\mathrm{u_k}} = \frac{\left(\mathrm{E_{u_k}}\right)_{\mathrm{AfterFailure}}}{\left(\mathrm{E_{u_k}}\right)_{\mathrm{BeforeFailure}}} \qquad (19)$$

Therefore: $s_d \in [0,1]$, with $s_d=1$ for no failure and $s_d=0$ for completely missing control surface.

5 Results

The performance of the neural controller has been evaluated through different sets of maneuvers.

The first set of maneuver is accomplished with prerecorded time histories of 56 seconds. The control action concerns short aileron, stabilator and rudder doublets and are devided into two successive sequences, from 0 to 24 sec and from 32 and 56 sec (Figure 3). Failure is scheduled at 24 sec, but the absence of the pilot-in-the-loop makes the failure a quasi-random event. In this second set of maneuver 8 different failures are considered, to evaluate the effects of partial missing control surfaces (Man. from #2 and #5) and locked surfaces at the current deflection (Man. from #6 and #9). Failures concern in turns the 4 surfaces: stabilators, ailerons, rudders and canards, as shown in Table 2 and

Table [3]. Comparison is made with the first 24 seconds of each maneuver (Man. # 1), which reflect the controller behaviour in nominal condition. The NN activity, reported in

Table [3] and Figure 4, is the difference between the command signals (δ_{lat}, δ_{lon}, δ_{dir}) calculated by the linear inverse model and those actually obtained by the neural inverse model. The NN activity is obviously supposed to increase when the aircraft is subjected to a failure event. Actually Figure 4 shows how the NN respond to compensate the aircraft deficiency, consistently with the kind of failure that occurs: the partial missing stabilator requests an increasing of the deflection mean value while the lockage implies wider deflection of the remaining effectors. Figure 5 shows the relative error for the three channels, roll, pitch and yaw, calculated as a percetage of the maximum value of the reference signal for Man. #4 and Man. #8. The tracking errors increase in post-failuire conditions but remain bounded in a very narrow range.

The second set of maneuvers concerns failures with the actuators locked at an imposed deflection, which is one of the most demanding failure event. Each maneuver, of 200 seconds, is carried out with the pilot-in-the-loop and consists of three phases where the state variables vary within a wide portion of the flight envelope:

- starting from a steady level flight at 6000 m and Mach = 0.75, three short doublets have been accomplished respectively with ailerons, stabilators and rudder;
- after 45 seconds there is a descent to 1000 m and Mach = 0.5 within 80 s;
- after the trim into the new flight condition, a set of doublets on the primary control surfaces has been performed in the same way as described above.

Referring to Table 4, Table 5 and Figure 6, Man. #10 is peformed in non failure condition. Man. #11 features a left stabilator lockage at -5 deg in t_{fl} = 30 sec. (before the first rudder doublet, as shown in Figure 7). Man. #12 refers to a right canard lockage at -5 deg in t_{fl} = 30 sec. Thus, this set of maneuvers shows up the combined effects of the failure and of the operative condition change (in terms of altitude and ground speed). shows that the tracking action is performed with very low errors for roll and pitch channels, while the yaw channel has always less desiderable peformace, due to the strong coupling between *p* and *r*. For Man. #11 and # 12 the tracking errors slightly increase, in particular for the pitch channel as far as Man. # 11 is concerned and for the yaw channel in Man. # 12, as failures affect the aerodynamic surfaces that contribute, respectively, to the pitch and roll angular rate.

Table 5 the integral of the control activity (ICA) for all the surfaces in terms of collective and differential stabilators, collective e differential ailerons, rudders, collective and differential canards. Obviously the control activity increase for all the three channels, apart from the surface directly aftected by the failure. This is due to the asymmetry of the failure which may introduce dynamic coupling effects and alteration of both force and moment setting up.

6. Conclusions

Performance analysis of the Predictor-Corrector neural controllor has been carried out in post-failure conditions. Different failure scenarios have been simulated according to an incresing level of workload for the NN controller: locked surface at the current deflection, missing surface and locked surface at an imposed deflection. Failures affect all the aerodynamic surfaces: stabilators, ailerons, rudder and canards. The neural controller has been tested both with simulations featuring the pilot-in-the-loop and with pre-recorded maneuvers. In all these situations, results demonstrate the capability of the neural controller of accomodating slight or hazardous damages with a very short transient.

Acknowledgements

Support for the authors has been provided through a grant from the Institute for Scientific Research (ISR).

References

[1] Annon., “Intelligent Flight Control: Advanced Concept Program – Final Report”, The Boeing Company, BOEING-STL 99P0040, May 1999.

[2] Rysdyk R.T., Calise A. J., “Fault Tolerant Flight Control via Adaptive Neural Network Augmentation”, *AIAA GN&C Conference*, Vol. 3, AIAA Reston, VA, 1998, pp.1722-1728.

[3] Kaneshige J., Bull J., Totah J.J., “Generic Neural Flight Control and Autopilot System”, *AIAA GN&C Conference*, [CD-ROM], AIAA Reston, VA, 2000.

[4] Gili P., Battipede M., “An Adaptive Neurocontroller for a Nonlinear Combat Aircraft Model”, *Journal of Guidance, Control, and Dynamics*, Vol. 24, No. 5, September-October 2001, pp. 910-917.

[5] Gili P., Battipede M., “A MIMO Neural Adaptive Autopilot for a Nonlinear Helicopter Model”, *AIAA GN&C Conference*, [CD-ROM], AIAA Reston, VA, 1999.

[6] Calise A. J., Lee S., Sharma M., “Direct Adaptive Reconfigurable Control of a Tailless Fighter Aircraft”, *AIAA GN&C Conference*, Vol. 1, AIAA Reston, VA, 1998, pp. 88-97.

[7] Calise A. J., Sharma M., "Adaptive Autopilot Design for Guided Munitions", *AIAA Journal of Guidance, Control and Dynamics,* Vol. 23, No. 5, 2000, pp. 837-843.

[8] Kaneshige J., Gundy-Burlet K., "Integrated Neural Flight and Propulsion Control System", AIAA *GN&C Conference*, [CD-ROM], AIAA Reston, VA, 2001.
[9] Norgaard M., "Neural Network Based System Identification Toolbox", *DTU-TR-97-E-851*, Department of Automation, Technical University of Denmark, Lyngby, June 1997, chap. 2, pp. 22-23.
[10] Ljung L., "System Identification: Theory for the User", *Prentice-Hall Inc*., Englewood Cliffs, New Jersey, 1987, pp. 71-72.
[11] Perhinschi M.G., Campa G., Napolitano M.R., Lando M., Massotti L., Fravolini M.L., "A Simulation Tool for On-line Real Time Parameter Identification", *AIAA MS&T Conference*, [CD-ROM], AIAA Reston, VA, 2002.
[12] Brumbaugh, R.W. "An Aircraft Model for the AIAA Controls Design Challenge", NASA CR 186019, Dec. 1991.
[13] Rauw M.O., "*FDC 1.2: A Simulink Toolbox for Flight Dynamics and Control Analysis*", Delft University of Technology, The Netherlands, 1998.
[14] "*Aviator Visual Design Simulator (AVDS) - User Manual*", Rassmussen Simulation Technologies, Ltd., October 2000.
[15] Napolitano M.R., Younghawn A., Seanor B., "A Fault Tolerant Flight Control System for Sensor and Actuator Failures using Neural Networks", Aircraft Design, Vol.3 No. 2, 2000, pp. 103-128.
[16] Perhinschi M.G., Campa G., Napolitano M.R., Lando M., Massotti L., Fravolini M.L., "Modeling and Simulation of Failures for Primary Control Surfaces", *AIAA MS&T Conference*, [CD-ROM], AIAA Reston, VA, 2002.

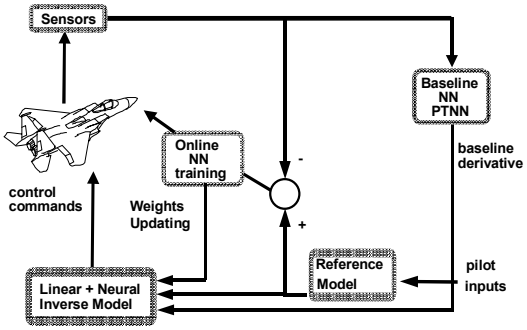

Figure 1 General Block Diagram of the IFCS F-15 *Gen-2* Program

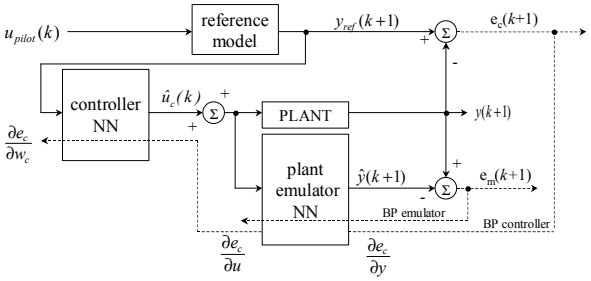

Figure 2 Predictor-Corrector scheme

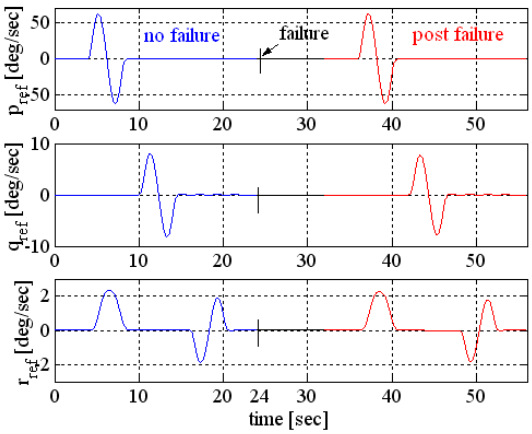

Figure 3 Reference signal for the first set of maneuvers

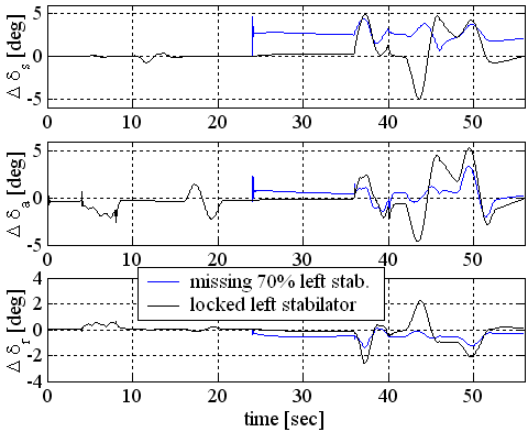

Figure 4 NN activity for Man. #2 and Man. #6

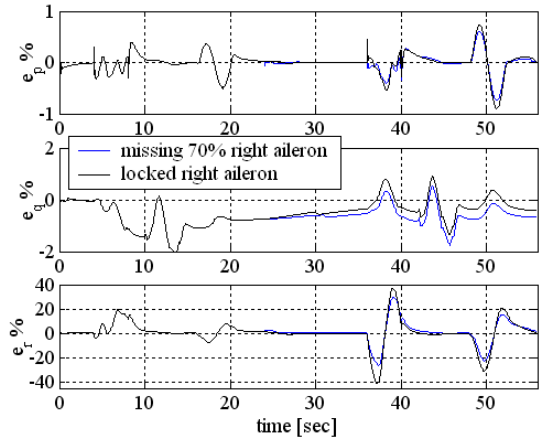

Figure 5 Relative errors for Man. #4 and Man. #8

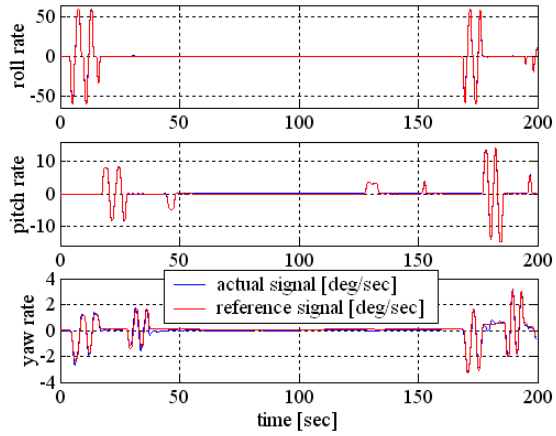

Figure 6 Man #10 (no failure)

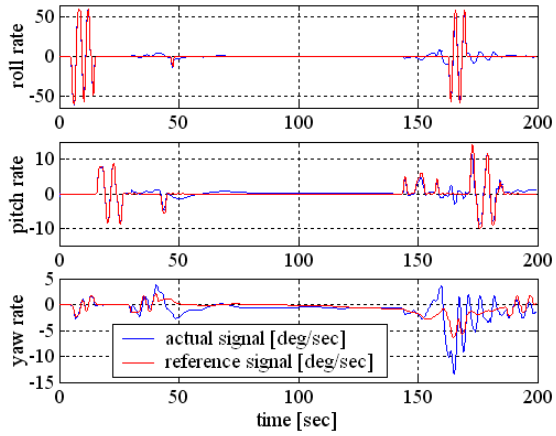

Figure 7 Man #11 (left stabilator lockage at -5 deg in t_{fl} = 30 sec)

Table 2 Tracking error for the first set of maneuvers

Tracking error		Mean error [rad/sec]			Std error [rad/sec]			Max error [rad/sec]		
		roll	pitch	yaw	roll	pitch	yaw	roll	pitch	yaw
Man. #1 - No failure		-7.05E-05	-1.05E-03	1.02E-03	1.77E-03	7.66E-04	2.06E-03	5.44E-03	2.95E-03	7.84E-03
missing surface	Man. #2 - left stab.	-1.69E-04	-1.80E-03	-8.34E-04	3.61E-03	2.57E-03	2.65E-03	1.07E-02	7.73E-03	9.96E-03
	Man. #3 - right can.	-3.01E-04	-3.92E-03	7.51E-03	3.49E-03	2.21E-03	2.90E-03	9.05E-03	6.87E-03	1.54E-02
	Man. #4 - right ail.	1.38E-03	-3.07E-03	7.59E-04	1.21E-02	6.20E-03	6.05E-03	3.48E-02	1.38E-02	1.78E-02
	Man. #5 - left rud.	-2.13E-04	-2.93E-03	6.87E-03	8.49E-03	3.63E-03	5.39E-03	2.53E-02	1.15E-02	1.90E-02
locked surface	Man. #6 - left stab.	-7.12E-05	-7.88E-04	3.97E-04	2.41E-03	5.38E-04	4.35E-03	7.93E-03	2.48E-03	1.21E-02
	Man. #7 - right can.	-4.06E-05	-3.15E-04	-2.13E-04	2.89E-03	5.76E-04	5.81E-03	9.66E-03	1.92E-03	1.66E-02
	Man. #8 - right ail.	1.22E-05	-3.29E-04	-4.50E-04	3.33E-03	6.27E-04	6.61E-03	9.29E-03	2.07E-03	1.65E-02
	Man. #9 - left rud.	1.24E-05	-7.21E-04	1.72E-04	2.80E-03	5.67E-04	4.74E-03	7.74E-03	2.51E-03	1.15E-02

Table 3 NN activity for the first set of maneuvers

NN activity		Mean value [rad]			Std value [rad]			Max value [rad]		
		$\Delta\delta_s$	$\Delta\delta_a$	$\Delta\delta_r$	$\Delta\delta_s$	$\Delta\delta_a$	$\Delta\delta_r$	$\Delta\delta_s$	$\Delta\delta_a$	$\Delta\delta_r$
Man. #1 - No failure		-3.46E-04	-9.21E-03	1.80E-03	2.87E-03	1.24E-02	2.81E-03	1.38E-02	4.56E-02	1.18E-02
missing surface	Man. #2 - left stab.	4.43E-02	5.88E-03	-8.85E-03	1.28E-02	1.69E-02	5.05E-03	7.73E-02	5.86E-02	2.40E-02
	Man. #3 - right can.	-1.56E-02	-4.52E-02	8.77E-03	6.02E-03	1.98E-02	5.29E-03	3.04E-02	9.41E-02	2.70E-02
	Man. #4 - right ail.	1.55E-02	4.77E-03	-5.15E-03	3.79E-02	3.93E-02	1.62E-02	8.81E-02	9.29E-02	4.60E-02
	Man. #5 - left rud.	-1.49E-02	-3.95E-02	1.16E-02	2.00E-02	5.14E-02	8.53E-03	5.79E-02	1.65E-01	3.89E-02
locked surface	Man. #6 - left stab.	1.03E-04	-6.31E-03	1.57E-03	2.78E-03	2.25E-02	2.35E-03	1.26E-02	5.95E-02	1.09E-02
	Man. #7 - right can.	1.92E-04	-3.18E-03	1.49E-03	2.76E-03	2.99E-02	2.17E-03	1.25E-02	7.89E-02	1.07E-02
	Man. #8 - right ail.	2.61E-04	-3.23E-03	5.94E-03	2.89E-03	1.83E-02	8.66E-03	1.29E-02	5.12E-02	4.24E-02
	Man. #9 - left rud.	1.51E-04	-5.50E-03	4.46E-03	2.89E-03	1.48E-02	6.36E-03	1.30E-02	5.14E-02	3.08E-02

Table 4 Tracking error for the second set of maneuvers

Tracking error	Mean error [rad/sec]			Std error [rad/sec]			Max error [rad/sec]		
	roll	pitch	yaw	roll	pitch	yaw	roll	pitch	yaw
Man. #10 - No failure	-6.15E-05	-1.73E-04	1.14E-03	1.02E-02	2.14E-03	2.33E-03	6.76E-02	1.48E-02	1.14E-02
Man. #11 - left stab.	2.30E-03	7.27E-03	-6.96E-03	3.78E-02	1.40E-02	1.52E-02	1.98E-01	1.06E-01	1.25E-01
Man. #12 - right can.	9.02E-05	-9.48E-03	1.36E-02	1.24E-02	7.07E-03	1.08E-02	7.37E-02	2.47E-02	5.83E-02

Table 5 Control activity for the second set of maneuvers

Integral Control Activity (ICA)	stabilators [rad/sec]		ailerons [rad/sec]		rudder [rad/sec]	canards [rad/sec]	
	collective	differential	collective	differential	collective	collective	differential
Man. #10 - No failure	3.91E+00	3.30E+00	0.00E+00	6.61E+00	3.48E+00	6.05E+00	2.66E+00
Man. #11 - left stab.	4.26E+00	2.86E+01	0.00E+00	3.50E+01	2.19E+01	6.88E+00	2.29E+01
Man. #12 - right can.	1.12E+01	1.31E+01	0.00E+00	2.61E+01	2.45E+01	1.83E+01	9.55E+00